JOURNAL OF SYNCHROTRON RADIATION
ISSN 1600-5775

Received 29 May 2019
Accepted 21 January 2020

Edited by A. F. Craievich, University of São Paulo, Brazil

Keywords: extended X-ray absorption fine structure; ultra-fast temperature measurement technology; anharmonic correlated Debye model; synchrotron radiation platform.

Supporting information: this article has supporting information at journals.iucr.org/s

Theoretical development and experimental validation on the measurement of temperature by extended X-ray absorption fine structure

Qing Ye,[a] Yun Hu,[a] Xiaoxi Duan,[a] Hao Liu,[a] Huan Zhang,[a] Chen Zhang,[a] Liang Sun,[a] Weiming Yang,[a] Wei Xu,[b] Quan Cai,[b] Zhebin Wang[a]* and Shaoen Jiang[a]*

[a]Laser Fusion Research Center, China Academy of Engineering Physics, Mianyang 621900, People's Republic of China, and [b]Beijing Synchrotron Radiation Facility, Institute of High Energy Physics, CAS, Beijing 100049, People's Republic of China. *Correspondence e-mail: zhebinw@vip.sina.com, jiangshn@vip.sina.com

A systematic investigation on the theoretical framework of the ultra-fast measurement of temperature by extended X-ray absorption fine structure (EXAFS) applied in laser-driven-compression experiments has been carried out and a new temperature measurement scheme based on the EXAFS cumulant expansion analysis and anharmonic correlated Debye model has been advanced. By considering the anharmonic effect of thermal vibration and avoiding the employment of the empirical model as well as parameters which have large inherent uncertainties in the temperature determination, this new scheme is theoretically more accurate than traditional ones. Then the performance of the new measurement scheme and traditional methods were validated on a synchrotron radiation platform by temperature-dependent EXAFS (TDEXAFS) experiments on Au, Fe, V and Ti; the results showed that the new scheme could provide the most accurate measured temperatures with much lower uncertainties. This accurate scheme gives a firmer physical ground to the EXAFS temperature measurement technique and can expect to be applied in laser-driven compression experiments and promote the development of matter state research at extreme conditions.

1. Introduction

Laser-driven compression technology, known for its unique ability to achieve far higher compressions than hydrostatic pressure and traditional dynamic pressure-loading technologies, has been utilized to continuously refresh the limit of artificial compression states of various materials (Smith *et al.*, 2007; Yaakobi *et al.*, 2008; Bradley *et al.*, 2009; Ping *et al.*, 2013; Wang *et al.*, 2014; Tateno *et al.*, 2010; Dubrovinsky *et al.*, 2000; Hemley *et al.*, 1997; Anzellini *et al.*, 2013). However, the extremely short duration (usually picoseconds to nanoseconds) of these states prevents the instantaneous state parameters from be measured by conventional methods. The technique of extended X-ray absorption fine-structure (EXAFS) spectroscopy, characterized by its ultra-fast response (femtoseconds) to the materials' structure and thermal motion (Dalba & Fornasini, 1997), has been utilized in laser-driven experiments since 1984 (Eason *et al.*, 1984). EXAFS describes the oscillation of the absorption coefficient along the X-ray energy in the range from 50 eV to 1000 eV above the absorption edge; this spectrum originates from the scattering of photoelectrons between the X-ray absorber and its neighbor atoms, which modulates the absorption cross-section of the absorber and leads to the oscillation behavior of

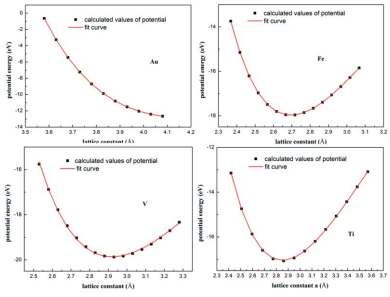

the absorption coefficient (Natoli *et al.*, 2003); temperature effects are reflected in the frequency (average interatomic distances) and amplitude of the EXAFS signals. By the efforts of Yaakobi *et al.* (2004) and Ping *et al.* (2013), the EXAFS experimental technique was established at the OMEGA laser-fusion facility, Los Alamos, USA. In these experiments, a short time-scale pulse (usually tens to hundreds of picoseconds) of continuum X-rays was produced by the bremsstrahlung radiation of a laser-driven target. Then the EXAFS signal which passed through the samples was recorded by imaging plates/CCD-detectors after being spectrally dispersed in a crystal spectrometer. With this EXAFS technique, Yaakobi and Ping attempted to measure the temperatures, densities (Yaakobi *et al.*, 2003, 2004) as well as identify the phase transitions of the compressed samples (Yaakobi *et al.*, 2005*a*,*b*) – the measured temperatures showed apparent differences with the results of hydrodynamic simulations in laser-shock of vanadium, titanium (Yaakobi *et al.*, 2004) and the quasi-isentropical compression of iron (Yaakobi *et al.*, 2008), and the measurement uncertainties of the temperature were generally considerable (Ping *et al.*, 2013).

Although the EXAFS technique has been widely applied in laser-driven experiments, there are still some problems concerning the basic limits of the EXAFS method. Firstly, it is a short-range-sensitive technique – only the microstructure in the range about 10 Å from the absorber atom can be solved from EXAFS, so it is insufficient to measure some quantities concerning long-range information such as density in these cases; X-ray diffraction (XRD) is an ideally complementary technique due to its long-range-sensitive features. Moreover, solving temperature from EXAFS will involve lattice dynamics models and EXAFS data analysis procedures – the rationality and applicability of these methods needs to be considered, especially in the high-temperature and high-pressure laser-compression condition. However, in Yaakobi's temperature measurement scheme, only the simplest harmonic approximation was employed for both lattice vibration model and EXAFS analysis procedure (Yaakobi *et al.*, 2003, 2004, 2005*a*,*b*). Actually, it has been realized that the thermal vibration of a crystal is essentially anharmonic due to the non-linear nature of the potential well in the crystal (Crozier & Seary, 1980), and this anharmonic effect will be enhanced by an increase of temperature (Van Hung *et al.*, 2003). Di Cicco *et al.* found that for AgBr crystal the anharmonic effects are important even at room temperature (Di Cicco *et al.*, 2000), so the EXAFS signal will deviate from the harmonic model prediction at sufficiently high temperatures (Van Hung *et al.*, 2003; Wenzel *et al.*, 1990; Frenkel & Rehr, 1993; Yokoyama, 1998). Neglecting the anharmonic components of thermal vibrations is inappropriate when dealing with EXAFS data of laser-driven compression in which the sample can be easily heated to 10^2–10^3 K or even higher by the X-rays, super thermal electrons, shock as well as compression (Yaakobi *et al.*, 2008).

In this work we advanced a new temperature measurement scheme by the combination of cumulant expansion method and anharmonic correlated Debye model; then a systematic experimental verification to check the reliability of the traditional EXAFS measurement method as well as our newly developed method was carried out, with the help of a high-brightness synchrotron radiation X-ray source, and EXAFS of Au, Fe, V and Ti were recorded in a series of determined temperatures. Then the temperatures were re-solved according to the new scheme and traditional schemes (Yaakobi's and Ping's methods). By comparing the measurement results with the actual temperatures, the measurement uncertainty and accuracy of our new scheme was shown to be superior to the other traditional methods.

This paper is organized as follows. Section 2 describes the theoretical framework of our new EXAFS measurement scheme; Section 3 presents the detailed calculation procedures for gold, iron, vanadium and titanium; Section 4 exhibits the synchrotron radiation platform's temperature-dependent EXAFS experimental results for the above-mentioned metals and a discussion about the temperature measurement results deduced from our new scheme as well as traditional ones; finally, concluding remarks are made in Section 5.

2. Theoretical framework

The quantitative parameterization of the EXAFS oscillation $\chi(k)$ can be expressed as follows (Lee *et al.*, 1981),

$$\chi(k) = \sum_j N_j B_j(k) \int \frac{\rho_j(r)}{r_j^2} \exp\left[-2r_j/\lambda(k)\right] \times \sin\left[2kr_j + \delta_j(k)\right] \mathrm{d}r_j, \quad (1)$$

where N_j is the number of neighbor atoms in the jth shell with a distance of r_j from the absorption atom, $B_j(k)$ and $\delta_j(k)$ are the backscattering amplitude and phase, respectively. $\lambda(k)$ is the mean free path of the scattered photoelectron, and $\rho_j(r)$ refers to the radial position distribution of atoms. With the harmonic approximation of the thermal vibration, formula (1) reduces to the standard harmonic form of EXAFS (Lee *et al.*, 1981),

$$\chi(k) = \sum_j N_j B_j(k) \exp\left[-2\sigma^2 k^2 - 2r_j/\lambda(k)\right] \times \sin\left[2kr_j + \delta_j(k)\right] / kr_j^2, \quad (2)$$

where σ^2 is the mean square relative displacement (MSRD) (also called the Debye–Wallor factor) which is in fact a quantity used to estimate the deviation of an atom position from equilibrium due to the harmonic component vibration.

Yaakobi *et al.* used experimental EXAFS data to fit formula (2). The fitted σ^2 has a quantitative relationship with temperature T according to the Debye model (Beni & Platzman, 1976), or Correlated Debye model (Sevillano *et al.*, 1979), and thus the temperature can be solved. However, both models contain the Debye temperature parameter Θ_D whose value is calculated using the Cowan's empirical model, though this model was reported to be not quantitatively reliable (More *et al.*, 1988). As mentioned above, it is inappropriate to deal with EXAFS data of laser-driven compression in a

harmonic scenario, thus Ping developed Yaakobi's method and introduced an anharmonic correction parameter σ_3 to the standard harmonic form of EXAFS (Ping *et al.*, 2013; Sevillano *et al.*, 1979; Tranquada & Ingalls, 1983); as σ_3 is a small quantity, its fit uncertainty is usually quite large and gives rise to a large measurement uncertainty for the temperature. This is the main reason why the uncertainty of the temperature for Fe as determined could reach about 70% (Ping *et al.*, 2013).

In our scheme, the cumulant expansion method (Bunker, 1983) has been employed in the EXAFS analysis, in which the natural logarithm of the Fourier transformation of the effective distribution function in formula (1) is expanded by the cumulants C_n,

$$\ln \hat{P}(\hat{r}, \gamma, k) = \sum_{n=0}^{\infty} \frac{(2ik)^n}{n!} C_n(\hat{r}, \gamma), \tag{3}$$

where $\hat{P}(\hat{r}, \gamma, k)$ is the Fourier transformation of $P(r,\gamma)$, $P(r, \gamma) = [\rho_1(r)/r^2]\exp(-2r\gamma)$, $\gamma = \lambda^{-1}$. By the introduction of C_n, the EXAFS signal $\chi(k)$ has the following expression,

$$\chi(k) = \sum_j N_j B_j(k) \frac{\exp(-2r_j\gamma)}{kr_j^2} \times \mathrm{Im}\left\{ \exp\left[2ikr_j + i\delta_j(k) + \sum_{n_j=2}^{\infty} \frac{(2ik)^{n_j}}{n_j!} C_{n_j} \right] \right\}. \tag{4}$$

It should be noted that the derivation of formula (4) has no harmonic approximation and the atoms' vibration (including anharmonic behavior) is described by C_n. In the second-order expansion, formula (4) reduces to the harmonic type of formula (2) and C_2 equals σ^2. Moreover, to the best of our knowledge the σ^2–T curves predicted by the anharmonic correlated Debye model (Van Hung *et al.*, 2010) agree very well with various experimental data (Greegor & Lytle, 1979; Yokoyama *et al.*, 1989; Pirog *et al.*, 2002), as compared with other theoretical models including the traditional Debye model and Correlated Debye model. Thus, to solve the temperature we employed the anharmonic correlated Debye model in which the second cumulant C_2 as a function of temperature has been deduced,

$$C_2 = -\frac{\hbar a}{\pi (M k_{\mathrm{eff}})^{1/2}} \int_0^{\pi/a} \sin\left(\frac{qa}{2}\right) \frac{1 + z(q)}{1 - z(q)} \, \mathrm{d}q, \tag{5}$$

where M refers to the atom's mass, a is the lattice constant,

$$z(q) = \exp\left\{ \frac{2\hbar\left[(k_{\mathrm{eff}}/M)\left|\sin(qa/2)\right|\right]^{1/2}}{k_{\mathrm{B}}T} \right\}$$

and k_{eff} is the effective local force constant of the anharmonic interatomic effective potential V_{eff},

$$V_{\mathrm{eff}}(x) \simeq \frac{1}{2} k_{\mathrm{eff}} x^2 + k_{3\mathrm{eff}} x^3 + k_{4\mathrm{eff}} x^4. \tag{6}$$

So one can use EXAFS data to fit formula (4), then the temperature T can be solved by the fitted σ_3 and formula (5), but the precondition is the knowledge of k_{eff}. However, reported values of k_{eff} in the literature are mainly obtained from various empirical models and are quite different from each other (Mohammed *et al.*, 1984; Abajingin, 2012; Lincoln *et al.*, 1967). Reliable determination of k_{eff} is a key problem in solving the correct temperature. Here we designed a procedure to calculate k_{eff} based on the quantum mechanical calculation and embedded atom potential method. Firstly, the potential energy curves of the unit cells were calculated from first-principle methods using the *Vienna Ab initio Simulation Package* (*VASP*) (Kresse & Hafner, 1993, 1994; Kresse & Furthmuller, 1996*a*,*b*); then the potential energy curve was fitted by the Morse potential (Girifalco & Weizer, 1958),

$$V_{\text{first principle}} = \sum V_{\mathrm{Morse}}, \qquad V_{\mathrm{Morse}} = D\left[\exp(-2\beta x) - 2\exp(-\beta x)\right], \tag{7}$$

where the sum goes through all atom pairs in the unit cell, D and β refer to the dissociation energy and the width of the potential, respectively, and x is the deviation of the instantaneous atom pair distance from its equilibrium. By fitting the first-principle calculated unit cell potential curves to formula (7) the parameters D and β can be obtained; then the embedded atom potential model can been employed to describe the relation between σ_3 and σ^2 (Van Hung & Rehr, 1997),

$$V_{\mathrm{eff}}(x) = V_{\mathrm{Morse}}(x) + \sum_{i=1,2} \sum_{j\neq 1} V_{\mathrm{Morse}}\left(\frac{\mu}{M_i} x \, \hat{\boldsymbol{R}}_{12} \cdot \hat{\boldsymbol{R}}_{ij}\right), \qquad \mu = \frac{M_1 M_2}{M_1 + M_2}. \tag{8}$$

The sum i is over absorbing and backscattering atoms, the sum j is over their neighbors, M_i is the ith atom mass, and $\hat{\boldsymbol{R}}_{ij}$ is the unit vector along the bond between the ith and jth atoms. The first term on the right concerns only absorbing and backscattering atoms and the second one describes the lattice contributions to pair interaction and depends on crystal structure type. Using formula (8) and the Taylor series expansion of the Morse potential around its equilibrium position,

$$V_{\mathrm{Morse}}(x) = D\left(-1 + \beta^2 x^2 - \beta^3 x^3 + \frac{7}{12}\beta^4 x^4 + \ldots\right),$$

the coefficient k_{eff} can be deduced as a function of D and β.

Compared with traditional EXAFS temperature measurement schemes, this newly developed scheme is theoretically superior at the following points. Firstly, by employing the cumulant expansion EXAFS analysis method and the anharmonic correlated Debye model the new scheme can determine the temperature more reasonably and accurately in the anharmonic scenario. Secondly, we have advanced a procedure to bridge the only parameter (namely the first-order force constant K_{eff}) in temperature determination with strict quantum mechanical calculation; this procedure can avoid the employment of unreliable empirical models as well as parameters which have large inherent uncertainties. Thirdly, in Yaakobi's method the temperature determination is directly dependent on the lattice constant; in the compression experiments the varied lattice constant of matter obtained

from EXAFS fit has a fitting uncertainty which will transform to and then increase the uncertainty of the temperature measurement. On the contrary our new scheme has the advantage of decoupling the lattice constant in the temperature determination, thus the measurement uncertainty can be reduced.

Table 1
Comparison of the theoretical optimized lattice constants and experimental lattice constants of gold, iron, vanadium and titanium.

	Experimental lattice constant	Theoretical lattice constant	Deviation
Gold	4.070 Å (Spreadborough & Christian, 1959)	4.165 Å	2.33%
Iron	2.856 Å (Davey, 1925)	2.795 Å	2.14%
Vanadium	3.027 Å (Colligan *et al.*, 2005)	2.989 Å	1.26%
Titanium	$a = b = 2.906$ Å, $c = 4.667$ Å (Novoselova *et al.*, 2004)	$a = b = 2.927$ Å, $c = 4.609$ Å	$a = b = 0.72\%$, $c = 1.24\%$

3. Calculation details on gold, iron, vanadium and titanium

In this work we applied our new EXAFS measurement scheme on four kinds of metal: gold, iron, vanadium and titanium. Here the necessary calculations to obtain the parameters D, β and $k_{\rm eff}$ for these four kinds of metals are presented.

The potential energies of a single unit cell of gold, iron, vanadium and titanium under periodic condition were calculated using *VASP* (Kresse & Hafner, 1993, 1994; Kresse & Furthmuller, 1996*a*,*b*). The exchange-correlation potential was described by the local density approximation in the form of the Perdew–Burke–Ernzerhof exchange model (Perdew *et al.*, 1996). The electronic wavefunctions were expanded using a plane-wave basis with an energy cutoff of 400 eV. Brillouin-zone integration was performed by using a 9 × 9 × 9 Monkhost–Pack k-points grid. Test calculations showed that using more k-points did not lead to any noticeable changes in the converged energy. To check the reliability of this calculation procedure the geometry optimizations of the four kinds of crystals were carried out and compared with the experimental values (Table 1).

Table 1 shows that our theoretical calculation scheme can accurately reproduce the lattice constants (with the deviation being no more than 2.33%), thus we assume that the calculation procedure can correctly and reliably describe the potential energy in the unit cells of the four metal crystals. We calculated potential energy curves for the four kinds of metals; these curves were then fitted by the Morse potential [formula (7)], and the fit results are shown in Fig. 1. The fitted Morse curves were found to match the first-principle calculated ones

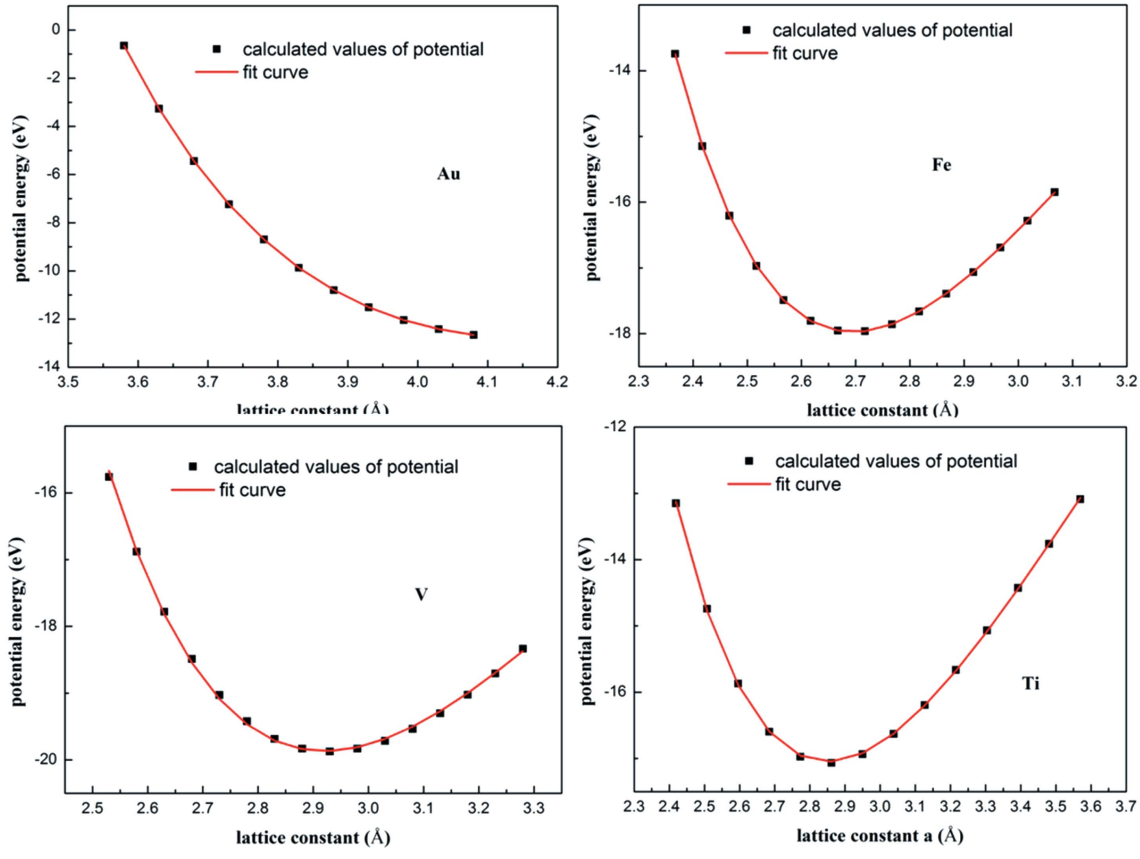

Figure 1
First-principle calculated potential energy curves as well as the fitted Morse curves for gold, iron, vanadium and titanium.

Table 2
Morse parameters and harmonic force constant $k_{\rm eff}$ of gold, iron, vanadium and titanium.

	Phase structure	D (eV)	β (Å^{-1})	Expression of $k_{\rm eff}$	Value of $k_{\rm eff}$ (N m^{-1})
Gold	Face-centered cubic	0.2254	1.2773	$5D\beta^2$	29.46
Iron	Body-centered cubic	0.6317	1.4107	$(11/3)D\beta^2$	73.84
Vanadium	Body-centered cubic	0.5871	1.1912	$(11/3)D\beta^2$	48.93
Titanium	Hexagonal close-packed	0.9323	0.8590	$5D\beta^2$	55.10

almost perfectly; actually, the typical residual sum of squares of these fittings was 2.94×10^{-5}, and the fit uncertainties were no more than 0.2%, thus we treated the fitted parameters D and β as specific values and ignored the influence of their uncertainties. The fitted parameters D, β and $k_{\rm eff}$ are listed in Table 2.

After the determination of the harmonic force constant $k_{\rm eff}$, the temperature T can be obtained with a given C_2 by numerically solving formula (5). However, the C_2 value has a fitting uncertainty typically from 5% to 15% according to our EXAFS data analysis. This uncertainty will propagate and influence the uncertainty of temperature T through the integral equation (5). We used a standard sampling method to determine the uncertainty of T: suppose there is a C_2 value fitted from EXAFS data with a fitting uncertainty of d, namely $C_2 \pm d$. We produced 1000 random values which have a Gaussian distribution around C_2 and have a standard deviation of d. The 1000 C_2 values were employed in equation (5) to solve 1000 temperature T values (numerically solve the integral equation 1000 times). Then we analyzed these 1000 temperature values statistically – the mean value of these 1000 T values is used as the final solved temperature value, and the standard deviation of these 1000 T values is used as the temperature's uncertainty.

Fig. 2 shows MSRD–T curves calculated using different methods. For the sake of clarity, Yaakobi's method (*i.e.* the uncorrelated Debye model; Yaakobi *et al.*, 2003) is labeled as method 1; the method from Yaakobi *et al.* (2004, 2005*a*,*b*) (*i.e.* the correlated Debye model) is labeled as method 2; Ping's method (the anharmonic modified Einstein model; Ping *et al.*, 2013) is labeled as method 3; and the present method is labeled as the 'Anharmonic correlated Debye model'. It can be seen that the different methods show distinct MSRD–T curves: method 1 and method 2 without anharmonic correction underestimate the MSRD compared with method 3 and our method, and the behavior of the curve in method 3 in the temperature range around 0 K is still linear while the other three curves approach a finite MSRD value. This difference can be attributed to the fundamental limitation of the Einstein model which assumes that all the atoms have the same vibration frequency (Poiarkova & Rehr, 1999). In summary, there are obvious differences between the four models in the MSRD–T curves, together with the differences in MSRD fitting procedures; it is foreseeable that the temperature measurement results of the four methods will be quite different. Thus systematical validating experiments need to be

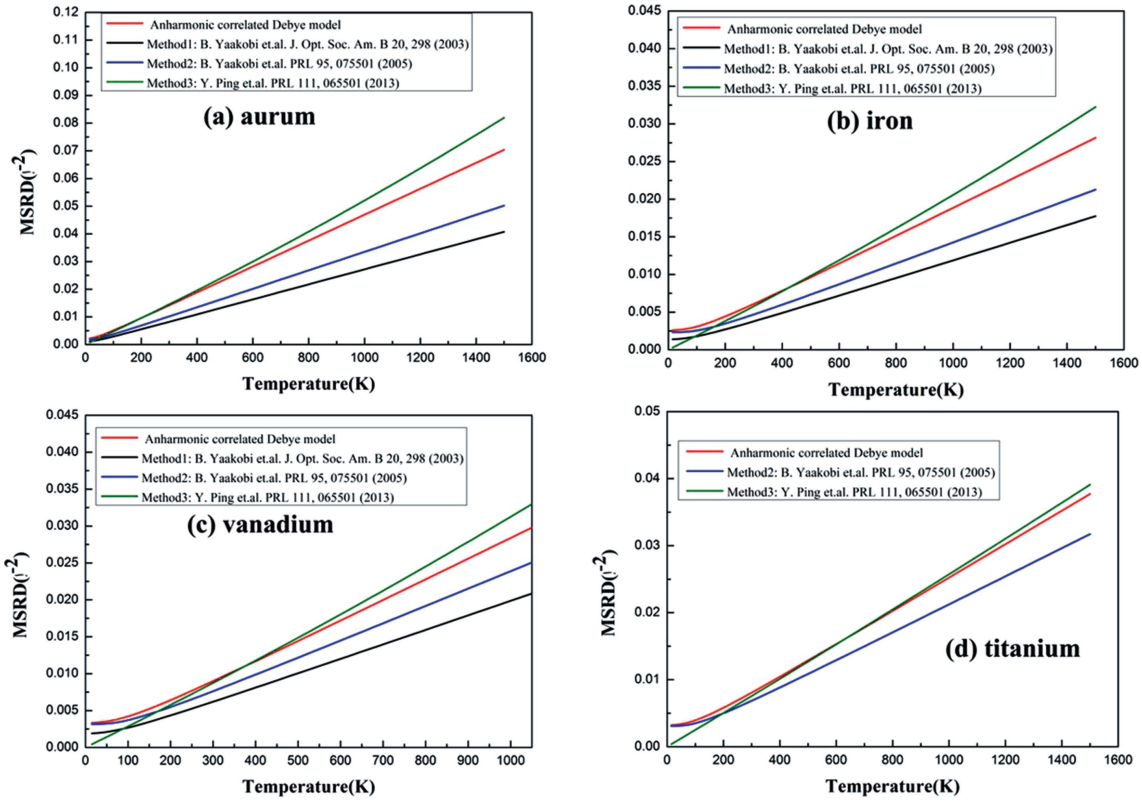

Figure 2
MSRD–temperature curves for the four methods as well as the measured temperatures of (*a*) gold, (*b*) iron, (*c*) vanadium and (*d*) titanium.

carried out to check the reliability and accuracy of our new temperature measurement scheme as well as traditional ones.

4. Temperature-dependent EXAFS experiments: results and discussion

A series of temperature-dependent EXAFS (TDEXAFS) experiments of gold, iron, vanadium and titanium were carried out at 1W1B XAFS station, Beijing Synchrotron Radiation Facility (BSRF). The temperatures of the samples were controlled by a heat system at a long time-scale (minutes) thermal equilibrium state and measured precisely by thermocouple with a measurement error of less than 10 K. The measured temperatures can be used as the criterion to identify the accuracy of different EXAFS measurement methods. These TDEXAFS spectra are shown in Fig. 3; the features of these spectra show no remarkable change except that the amplitude of the EXAFS oscillations decreases with increasing temperature, so we indicate there is no sign of phase transition and only changes of thermal disordering were observed in all experiments.

These TDEXAFS spectra were then employed to solve the temperatures according to our newly developed scheme, Yaakobi's methods as well as Ping's method. The measured temperatures with error bars and actual temperatures are shown in Fig. 4. The figure clearly shows that the temperature deduced using our new measurement scheme is remarkably consistent with the actual temperatures for all samples, while the measurement results of method 1 and method 2 are apparently in discrepancy with the actual temperatures. The performance of method 3 is good when measuring the temperature of iron [Fig. 3(*b*)] but rather poor when dealing with gold [Fig. 3(*a*)]. The comparison shows that our new temperature measurement scheme is much more reliable and accurate than the other traditional methods in the experimental temperature range. (Details of the temperature measurement of methods 1, 2 and 3 are provided in the supporting information.)

The fitted results based on fourth-, third- and second-order cumulant expansion are compared in Table 3. The measured temperatures based on the four methods are compared in Table 4. Here we underline that the cumulants may become rapidly unstable due to the strong statistical correlations among odd (or even) cumulants. Truncating the series at any order higher than the second (which corresponds to the Gaussian limit) is somewhat arbitrary and may lead to errors in the results (Filipponi, 2001). The second-order cumulants (namely σ^2) fitted from high-order expansion of formula (4) need to be carefully examined, so we independently evaluated σ^2 by carrying out the molecular dynamics (MD) simulations of the thermal motions for the four kinds of metals at different temperatures and standardized atmosphere (1 bar), and reproduced the σ^2 from the MD simulation trajectories. The good agreement between the EXAFS-fitted σ^2 values and the MD simulation reproduced σ^2 values suggests that this cumulant expansion method can obtain meaningful and reliable C_2 (σ^2) values, at least for Au, Fe, V and Ti crystals in our experimental temperature range. (A detailed introduction of

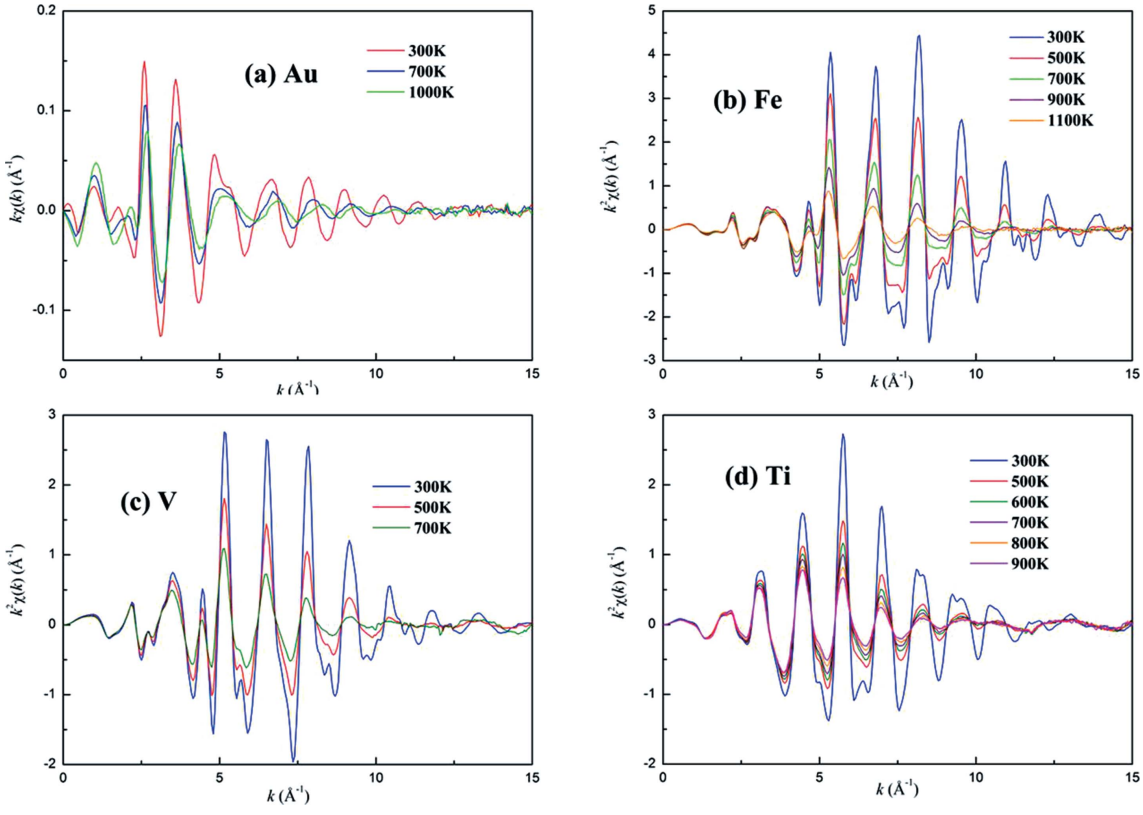

Figure 3
The k^n-weighted EXAFS signal along with photoelectron wavenumber k of (*a*) gold, (*b*) iron, (*c*) vanadium and (*d*) titanium at different temperatures.

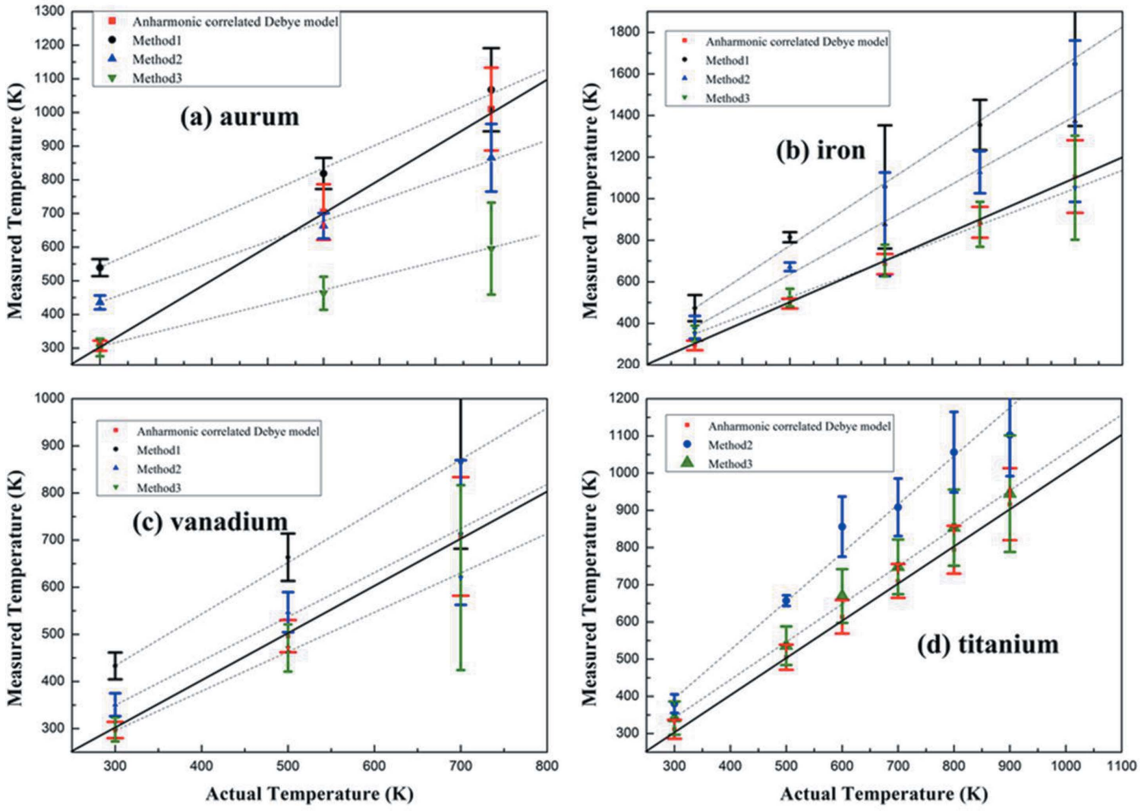

Figure 4
The measured temperatures for (*a*) gold, (*b*) iron, (*c*) vanadium and (*d*) titanium. The black lines are composed of points for which the measured temperature equals the actual temperature.

our MD simulation procedures and comparison between simulation results and cumulant expansion results can be found in the supporting information.)

When dealing with the EXAFS spectra of gold at 700 K and 1000 K we attempted to expand the fit formula (4) to the fourth-order cumulant C_4. It is noted that the fitted values of C_2 were different from their counterparts of the third-order cumulant expansion and ordinary fit [formula (2)]. The correct temperatures can only be deduced by the C_2 fitted from the fourth-order cumulant expansion, whereas for other metals the correct temperatures can be deduced by the fitted C_2 from the third-order cumulant expansion. This phenomenon is rather peculiar since there is a discrepancy of about 50% between the C_2 values fitted from the fourth-order expansion and the third-order expansion (see Table 3, where the fourth-order fit gives a C_2 value of 3.31×10^{-2} Å^2 while the third-order fit gives 2.21×10^{-2} Å^2). According to our experience the C_2 value should not be so sensitive to the cumulant expansion order, so the origin of this phenomenon still needs further investigation. A possible explanation is as follows. The Debye temperature Θ_D of gold is rather low compared with Θ_D of iron, vanadium and titanium (for Au, Θ_D = 165 K; for Fe, 470 K; for V, 380 K; for Ti, 420 K) [these values of Debye temperatures were extracted from Kun (1991)]. It was known that the anharmonic effect becomes remarkable at temperatures adequately higher than Θ_D (Van Hung *et al.*, 2014; Fultz, 2009). Accordingly, for gold, owing to its low Θ_D, the anharmonic effect is too strong to be correctly described by only the third-order cumulant expansion, and the fourth-order cumulant needs to be employed when dealing with gold's EXAFS at 700 K and 1000 K. However, the addition of the fourth-order cumulant in the EXAFS fit will increase the fitting uncertainty of C_2 (see Table 3), so to obtain the correct C_2 and ensure the measurement accuracy we have to compromise on the uncertainty. The largest temperature measurement uncertainty of our new scheme can be seen for 1000 K gold of 16.20% (Table 4), which is acceptable compared with other temperature measurement works in laser-driven experiments (Smith *et al.*, 2007; Ping *et al.*, 2013; Yaakobi *et al.*, 2003, 2004). Moreover, we noted that the uncertainty of C_3 is much larger than for C_2 in both the fourth-order and third-order cumulant expansion (see Table 3; even the smallest uncertainty of C_3 is 52.51%). As mentioned above, it is difficult to accurately obtain C_3 by EXAFS fit. The employment of C_3 in the temperature determination will increase the uncertainty of measurement. For instance, it can be seen from Table 4 that Ping's method (method 3) has introduced σ_3 (namely C_3) in the temperature determination and its measurement uncertainty is larger than for the other three methods. As shown in Table 4 and Fig. 3, the largest measurement deviation in our new method is only 3.89%; it is obvious that our new temperature determination scheme is much more accurate than other methods. Meanwhile the measured uncertainty of the new scheme is smaller than for Ping's method and comparable with Yaakobi's methods, though we have employed more parameters in the EXAFS fit (σ_3 and σ_4).

Table 3
Fitted results of fourth-order cumulant expansion, third-order cumulant expansion and ordinary fit for gold, iron, vanadium and titanium.

		Cumulant expansion (to fourth order)			Cumulant expansion (to third order)		Ordinary fit
	T	σ^2 (Å^2)	σ_3 (Å^3)	σ_4 (Å^4)	σ^2 (Å^2)	σ_3 (Å^3)	σ^2 (Å^2)
Au	300 K				1.46×10^{-2} ± 5%	2.65×10^{-4} ± 128%	1.47×10^{-2} ± 5%
	700 K	3.31×10^{-2} ± 12%	1.81×10^{-4} ± 187%	3.91×10^{-4} ± 32%	2.21×10^{-2} ± 6%	2.39×10^{-4} ± 249%	2.23×10^{-2} ± 6%
	1000 K	4.74×10^{-2} ± 16%	1.52×10^{-3} ± 86%	8.06×10^{-4} ± 75%	2.90×10^{-2} ± 13%	6.84×10^{-4} ± 245%	2.89×10^{-2} ± 12%
Fe	300 K				5.98×10^{-3} ± 7%	-2.59×10^{-4} ± 53%	5.74×10^{-3} ± 13%
	500 K				9.55×10^{-3} ± 4%	-1.07×10^{-4} ± 150%	9.70×10^{-3} ± 3%
	700 K				1.30×10^{-2} ± 7%	-4.70×10^{-5} ± 494%	1.25×10^{-2} ± 8%
	900 K				1.67×10^{-2} ± 8%	1.48×10^{-4} ± 190%	1.60×10^{-2} ± 9%
	1100 K				2.08×10^{-2} ± 16%	4.90×10^{-4} ± 127%	1.95×10^{-2} ± 18%
V	300 K				8.90×10^{-3} ± 5%	2.52×10^{-4} ± 53%	8.75×10^{-3} ± 6%
	500 K				1.43×10^{-2} ± 6.58%	5.27×10^{-4} ± 54%	1.33×10^{-2} ± 7%
	700 K				2.02×10^{-2} ± 17%	1.38×10^{-3} ± 75%	1.72×10^{-2} ± 21%
Ti	300 K				8.34×10^{-3} ± 7%	-2.11×10^{-4} ± 242%	8.45×10^{-3} ± 6%
	500 K				1.30×10^{-2} ± 6%	-4.32×10^{-4} ± 106%	1.41×10^{-2} ± 2%
	600 K				1.57×10^{-2} ± 7%	-1.10×10^{-3} ± 62%	1.82×10^{-2} ± 9%
	700 K				1.80×10^{-2} ± 6%	-6.94×10^{-4} ± 100%	1.93×10^{-2} ± 8%
	800 K				2.01×10^{-2} ± 8%	-1.24×10^{-3} ± 76%	2.24×10^{-2} ± 10%
	900 K				2.32×10^{-2} ± 10%	-5.11×10^{-4} ± 289%	2.34×10^{-2} ± 10%

5. Conclusion

The theoretical frameworks of current temperature measurement schemes by EXAFS still have limitations such as not sufficiently considering the anharmonic components of thermal vibrations, employing unreliable empirical models and parameters with large uncertainties in the temperature determination. Moreover, the systematic experimental work to evaluate the reliability and accuracy of current measurement schemes has not been reported yet. In this work, we developed a new temperature measurement scheme by combination of EXAFS cumulant expansion analysis and the anharmonic correlated Debye model. This scheme has considered the anharmonic effect of an atom's vibration which has been proved to be important in the high-temperature range; the only parameter (namely the first-order force constant $K_{\rm eff}$) in this new scheme can be deduced from strict quantum mechanical calculation. Meanwhile, features avoiding the empirical model and decoupling lattice constant in the temperature determination make it physically more accurate than traditional methods. Moreover, we carried out TDEXAFS experiments of gold, iron, vanadium and titanium at various temperatures on a synchrotron radiation platform. The TDEXAFS experimental data have been employed to measure the temperatures according to our new scheme as well as traditional ones. The measurement results show that our scheme is the best among the existing methods, with highest precision and rather low measurement uncertainty. This new EXAFS temperature measurement scheme, with experimental validation of its reliability and accuracy, can expect to be applied on a laser-driven experimental platform as it provides more reliable measurement results for the matter state research under extreme conditions.

Finally, to avoid possibly misleading the readers, we emphasize here that the new EXAFS temperature measurement scheme is only available for crystal samples (it is invalid in liquid or warm-density state or plasma), and a key problem of utilizing this scheme is the poorer quality of the EXAFS signal from ultra-fast measurement compared with long-timescale recorded EXAFS. We are making efforts to improve the EXAFS experimental technique and enhance the signal-to-noise ratio in our laser-compression facility.

6. Related literature

The following references, not cited in the main body of the paper, have been cited in the supporting information: Foiles *et al.* (1986); Mendelev *et al.* (2003, 2016); Olsson (2009); Plimpton (1995); Stern *et al.* (1991).

Table 4
Temperature measurement results of gold, iron, vanadium's and titanium.

		Method 1		Method 2		Method 3		New method	
	Actual temperature (Ta)	Measured result	Deviation from Ta	Measured result	Deviation from Ta	Measured result	Deviation from Ta	Measured result	Deviation from Ta
Au	300 K	539 K ± 5%	80%	436k ± 5%	45%	302 K ± 9%	1%	308 K ± 5%	3%
	700 K	819 K ± 6%	17%	663k ± 6%	5%	463 K ± 13%	34%	704 K ± 12%	1%
	1000 K	1068 K ± 12%	7%	865k ± 12%	13%	595 K ± 23%	40%	1010 K ± 16%	1%
Fe	300 K	473 K ± 13%	58%	381 K ± 14%	27%	351 K ± 11%	17%	294 K ± 8%	2%
	500 K	814 K ± 3%	63%	672 K ± 3%	34%	524 K ± 8%	5%	495 K ± 5%	1%
	700 K	1056 K ± 8%	51%	876 K ± 8%	24%	702 K ± 11%	1%	685 K ± 7%	2%
	900 K	1354 K ± 9%	50%	1127 K ± 9%	25%	877 K ± 12%	3%	886 K ± 8%	2%
	1100 K	1647 K ± 18%	50%	1372 K ± 18%	25%	1053 K ± 24%	4%	1106 K ± 16%	1%
V	300 K	433 K ± 7%	44%	351 K ± 7%	17%	298 K ± 9%	1%	297 K ± 6%	1%
	500 K	664 K ± 8%	33%	547 K ± 8%	9%	471 K ± 11%	6%	496 K ± 7%	1%
	700 K	865 K ± 21%	24%	716 K ± 21%	2%	620 K ± 32%	11%	708 K ± 18%	1%
Ti	300 K			380 K ± 7%	27%	342 K ± 13%	14%	312 K ± 8%	4%
	500 K			657 K ± 2%	31%	536 K ± 10%	7%	505 K ± 7%	1%
	600 K			856 K ± 9%	43%	670 K ± 11%	12%	614 K ± 7%	2%
	700 K			908 K ± 9%	30%	748 K ± 10%	7%	710 K ± 6%	1%
	800 K			1056 K ± 10%	32%	853 K ± 12%	7%	794 K ± 8%	1%
	900 K			1103 K ± 10%	23%	945 K ± 17%	5%	916 K ± 11%	2%

Acknowledgements

We would like to thank Professor Nguyen Van Hung of University of Science, VNU-Hanoi, for his qualified support on lattice dynamics.

Funding information

This work is supported by Science Challenge Project, No. TZ2016001, National Natural Science Foundation of China, No. 11704351, and National Natural Science Foundation of China, No. 11805183.

References

Abajingin, D. D. (2012). *Adv. Phys. Theor. Appl.* **8**, 36–44.
Anzellini, S., Dewaele, A., Mezouar, M., Loubeyre, P. & Morard, G. (2013). *Science*, **340**, 464–466.
Beni, G. & Platzman, P. M. (1976). *Phys. Rev. B*, **14**, 1514–1518.
Bradley, D. K., Eggert, J. H., Smith, R. F., Prisbrey, S. T., Hicks, D. G., Braun, D. G., Biener, J., Hamza, A. V., Rudd, R. E. & Collins, G. W. (2009). *Phys. Rev. Lett.* **102**, 075503.
Bunker, G. (1983). *Nucl. Instrum. Methods Phys. Res.* **207**, 437–444.
Colligan, M., Lee, Y., Vogt, T., Celestian, A. J., Parise, J. B., Marshall, W. G. & Hriljac, J. A. (2005). *J. Phys. Chem. B*, **109**, 18223–18225.
Crozier, E. D. & Seary, A. J. (1980). *Can. J. Phys.* **58**, 1388–1399.
Dalba, G. & Fornasini, P. (1997). *J. Synchrotron Rad.* **4**, 243–255.
Davey, W. P. (1925). *Phys. Rev.* **25**, 753–761.
Di Cicco, A., Taglienti, M., Minicucci, M. & Filipponi, A. (2000). *Phys. Rev. B*, **62**, 12001–12013.
Dubrovinsky, L. S., Saxena, S. K., Dubrovinskaia, N. A., Rekhi, S. & Le Bihan, T. (2000). *Am. Mineral.* **85**, 386–389.
Eason, R. W., Bradley, D. K., Kilkenny, J. D. & Greaves, G. N. (1984). *J. Phys. C.: Solid State Phys.* **17**, 5067–5074.
Filipponi, A. (2001). *J. Phys. Condens. Matter*, **13**, R23–R60.
Foiles, S. M., Baskes, M. I. & Daw, M. S. (1986). *Phys. Rev. B*, **33**, 7983–7991.
Frenkel, A. I. & Rehr, J. J. (1993). *Phys. Rev. B*, **48**, 585–588.
Fultz, B. (2009). *Vibrational Thermodynamics of Materials*, California Institute of Technology, W. M. Keck Laboratory, Pasadena, CA, USA.
Girifalco, L. A. & Weizer, V. G. (1958). *Phys. Rev.* **114**, 687–690.
Greegor, R. B. & Lytle, F. W. (1979). *Phys. Rev. B*, **20**, 4902–4907.
Hemley, R. J. (1997). *Science*, **276**, 1242–1245.
Kresse, G. & Furthmüller, J. (1996*a*). *Comput. Mater. Sci.* **6**, 15–50.
Kresse, G. & Furthmüller, J. (1996*b*). *Phys. Rev. B*, **54**, 11169–11186.
Kresse, G. & Hafner, J. (1993). *Phys. Rev. B*, **48**, 13115–13118.
Kresse, G. & Hafner, J. (1994). *Phys. Rev. B*, **49**, 14251–14269.
Kun, H. (1991). *Solid State Physics*. Higher Education Press.
Lee, P. A., Citrin, P. H., Eisenberger, P. & Kincaid, B. M. (1981). *Rev. Mod. Phys.* **53**, 769–806.
Lincoln, R. C., Koliwad, K. M. & Ghate, P. B. (1967). *Phys. Rev.* **157**, 463–466.
Mendelev, M. I., Han, S., Srolovitz, D. J., Ackland, G. J., Sun, D. Y. & Asta, M. (2003). *Philos. Mag.* **83**, 3977–3994.
Mendelev, M. I., Underwood, T. L. & Ackland, G. J. (2016). *J. Chem. Phys.* **145**, 154102.
Mohammed, K., Shukla, M. M., Milstein, F. & Merz, J. L. (1984). *Phys. Rev. B*, **29**, 3117–3126.
More, R. M., Warren, K. H., Young, D. A. & Zimmerman, G. B. (1988). *Phys. Fluids*, **31**, 3059.
Natoli, C. R., Benfatto, M., Della Longa, S. & Hatada, K. (2003). *J. Synchrotron Rad.* **10**, 26–42.
Novoselova, T., Malinov, S., Sha, W. & Zhecheva, A. (2004). *Mater. Sci. Eng. A*, **371**, 103–112.
Olsson, P. A. T. (2009). *Comput. Mater. Sci.* **47**, 135–145.
Perdew, J. P., Burke, K. & Ernzerhof, M. (1996). *Phys. Rev. Lett.* **77**, 3865–3868.
Plimpton, S. (1995). *J. Comput. Phys.* **117**, 1–19.
Ping, Y., Coppari, F., Hicks, D. G., Yaakobi, B., Fratanduono, D. E., Hamel, S., Eggert, J. H., Rygg, J. R., Smith, R. F., Swift, D. C., Braun, D. G., Boehly, T. R. & Collins, G. W. (2013). *Phys. Rev. Lett.* **111**, 065501.
Pirog, I. V., Nedoseikina, T. I., Zarubin, I. A. & Shuvaev, A. T. (2002). *J. Phys. Condens. Matter*, **14**, 1825–1832.
Poiarkova, A. V. & Rehr, J. J. (1999). *Phys. Rev. B*, **59**, 948–957.
Sevillano, E., Meuth, H. & Rehr, J. J. (1979). *Phys. Rev. B*, **20**, 4908–4911.
Smith, R. F., Lorenz, K. T., Ho, D., Remington, B. A., Hamza, A., Rogers, J., Pollaine, S., Jeon, S., Nam, Y. & Kilkenny, J. (2007). *Astrophys. Space Sci.* **307**, 269–272.
Spreadborough, J. & Christian, J. W. (1959). *J. Sci. Instrum.* **36**, 116–118.

Stern, E. A., Līvņš, P. & Zhang, Z. (1991). *Phys. Rev. B*, **43**, 8850–8860.
Tateno, S., Hirose, K., Ohishi, Y. & Tatsumi, Y. (2010). *Science*, **330**, 359–361.
Tranquada, J. M. & Ingalls, R. (1983). *Phys. Rev. B*, **28**, 3520–3528.
Van Hung, N. & Rehr, J. J. (1997). *Phys. Rev. B*, **56**, 43–46.
Van Hung, N., Duc, N. B. & Frahm, R. R. (2003). *J. Phys. Soc. Jpn*, **72**, 1254–1259.
Van Hung, N., Trung, N. B., Duc, N. B., Son, D. D. & Tien, T. S. (2014). *J. Phys. Sci. Appl.* **4**, 43–49.
Van Hung, N., Trung, N. B. & Kirchner, B. (2010). *Physica B*, **405**, 2519–2525.
Wang, J., Smith, R. F., Coppari, F., Eggert, J. H., Boehly, T. R., Collins, G. W. & Duffy, T. S. (2014). *J. Phys. Conf. Ser.* **500**, 062002.
Wenzel, L., Arvanitis, D., Rabus, H., Lederer, T., Baberschke, K. & Comelli, G. (1990). *Phys. Rev. Lett.* **64**, 1765–1768.
Yaakobi, B., Boehly, T. R., Meyerhofer, D. D., Collins, T. J. B., Remington, B. A., Allen, P. G., Pollaine, S. M., Lorenzana, H. E. & Eggert, J. H. (2005*a*). *Phys. Rev. Lett.* **95**, 075501.
Yaakobi, B., Boehly, T. R., Meyerhofer, D. D., Collins, T. J. B., Remington, B. A., Allen, P. G., Pollaine, S. M., Lorenzana, H. E. & Eggert, J. H. (2005*b*). *Phys. Plasmas*, **12**, 092703.
Yaakobi, B., Boehly, T. R., Sangster, T. C., Meyerhofer, D. D., Remington, B. A., Allen, P. G., Pollaine, S. M., Lorenzana, H. E., Lorenz, K. T. & Hawreliak, J. A. (2008). *Phys. Plasmas*, **15**, 062703.
Yaakobi, B., Marshall, F. J., Boehly, T. R., Town, R. P. J. & Meyerhofer, D. D. (2003). *J. Opt. Soc. Am. B*, **20**, 238.
Yaakobi, B., Meyerhofer, D. D., Boehly, T. R., Rehr, J. J., Remington, B. A., Allen, P. G., Pollaine, S. M. & Albers, R. C. (2004). *Phys. Rev. Lett.* **92**, 095504.
Yokoyama, T. (1998). *Phys. Rev. B*, **57**, 3423–3432.
Yokoyama, T., Satsukawa, T. & Ohta, T. (1989). *Jpn. J. Appl. Phys.* **28**, 1905–1908.